

PDF CALCULATIONS FOR SWIRLING FLOWS

M. S. Anand
Allison Gas Turbine Division
General Motors Corporation
Indianapolis, Indiana

S. B. Pope[†]
Sibley School of Mechanical and Aerospace Engineering
Cornell University
Ithaca, New York

H. C. Mongia^{*}
Allison Gas Turbine Division
General Motors Corporation
Indianapolis, Indiana

Abstract

The demonstrated advantages of the probability density function (pdf) method over conventional turbulence models have made it a most promising tool for computing the complex flow fields, involving turbulence, mixing, and chemical reaction, encountered in engineering applications, especially practical combustion devices. There are three aspects to the present study: i) swirling flows, an essential ingredient in practical combustion devices, have not been studied previously with the pdf method. In the present study, the pdf method is extended and applied to a coaxial swirling jet flow and the results are compared with detailed experimental data; ii) the recently developed stochastic dissipation model (Pope and Chen, 1990), hitherto applied only to homogeneous turbulence and self-similar flows, is applied to and validated for a general developing shear flow as represented by the coaxial swirling jet flow considered. The results are also compared against computations using a previous model based on the mean dissipation (Anand, Pope, and Mongia 1989); iii) detailed velocity statistics, conditional upon the jet from which the fluid originated, are calculated and compared against measurements, demonstrating that, in addition to other advantages, the pdf method can provide considerably more description of the flow than conventional models, and yet is computationally tractable. The results are in very good agreement with data.

Introduction

Several previous studies, most of them recently reviewed by Pope,¹ have established the probability density function (pdf) method as a prime candidate for computing complex turbulent flow fields in which mixing and reaction are occurring. Unlike the currently used turbulence models, the most important processes, namely convection (by both mean and fluctuating velocities) and reaction, appear in closed form in the joint velocity-composition pdf method and need not be modeled.² The conventional turbulence models such as $k-\epsilon$ and Reynolds-stress models (RSMs), based on Reynolds-averaged equations, use gradient diffusion models for turbulent transport (convection by fluctuating velocities). More importantly, the models are incapable of treating finite-rate multi-step reactions. The ability to treat these reactions is essential for computing, understanding, and controlling pollutant emissions that has become ever-more important for current and future land-based and aerospace applications. The present study is another step in the development of the pdf method as a design and analysis tool for practical systems.

The pdf method has been applied to a number of reacting and nonreacting flows including two-dimensional recirculating flows^{3,4} and, in conjunction with a Reynolds-averaged finite-volume method, to two- and three-dimensional time-dependent flows.^{5,6} Swirling flows (flows with appreciable bulk swirl) are an essential feature in many practical combustors such as gas turbine combustors. Swirling flows have not been studied previously with the pdf method, although there are no theoretical restrictions for applying the pdf

^{*} Member, AIAA

[†] Associate Fellow, AIAA

method for such flows. In the present study, the necessary extensions to the solution algorithm are made to include the treatment of swirl. For the boundary-layer type flow under consideration, a salient feature of this extension is the inclusion of the mean axial pressure gradient in the calculations.

It is well known that the $k-\epsilon$ model, which is the most widely used turbulence model, is unsatisfactory for swirling flows⁷ due to effects of streamline curvature, although the model performs reasonably well for nonswirling jet flows. Several modifications to the $k-\epsilon$ model to account for curvature effects, through corrections based on the Richardson number, have been investigated and reported in the literature. The corrections are typically made through the equation for mean dissipation as a means of correcting the turbulent transport. However, these modifications have not proved to be uniformly successful over a range of swirling flows. In this context, it is necessary to verify the performance of the pdf method for swirling flows.

A serious deficiency in the joint velocity-composition pdf method is that the joint pdf contains no information on the time or length scales of the turbulent motions. However, given the time scale information, the method provides a complete one-point description of the joint velocity-composition statistics. For several shear flows, previous studies⁸⁻¹¹ have assumed the turbulent time scale to be uniform across the flow. The turbulent time scale is defined to be the ratio of the turbulent kinetic energy to the mean dissipation rate ($\tau = k / \langle \epsilon \rangle$). The assumption of a uniform time scale is not valid in the developing regions of the shear flow.¹² The alternatives have been to solve³⁻⁶ the standard model equation for $\langle \epsilon \rangle$,^{13,14} or to solve a model equation^{12,15} for the turbulent frequency $\langle \omega \rangle = 1/\tau$.

The model developed recently by Pope and Chen¹⁶ eliminates the need to supply the time scale information to the pdf equation. This is done by considering the joint pdf of velocity, composition, and the instantaneous dissipation ϵ . In addition to effecting complete closure of the joint pdf equation, the inclusion of ϵ in the joint pdf leads to more realistic modeling. For example, the model allows for multiple time scales rather than a single mean time scale, accounts for internal intermittency, has potential to account for large scale structures, and better accounts for the influence of the origin and history of the fluid particles on the local turbulent structure. The model was constructed with refer-

ence to known and computed¹⁷ (by direct numerical simulations) properties of homogeneous turbulence. The model was extended by Pope¹⁸ to inhomogeneous turbulence and validated against several self-similar flows. An attempt to validate the model for a piloted jet diffusion flame by Norris and Pope¹⁹ was not very successful due to the complexities and uncertainties in the flow studied. In the present study, the model is validated against benchmark quality data of Takahashi et al²⁰ for a coaxial swirling jet flow.

A unique feature of the laser Doppler velocimeter (LDV) measurements of Takahashi et al²⁰ is that conditional velocity statistics are measured by seeding individual jets one at a time. This eliminates issues of velocity bias in the measurements. Conditional turbulent correlations up to fourth order have been reported. These conditional correlations are easily computed in the pdf method, and the comparisons against data serve to verify that turbulent transport is indeed accurately calculated in the pdf method.

The Joint pdf Method

A brief description of the method pertinent to the present study is presented here. More details can be obtained from previous studies.^{2,12,16,18}

The equation for the evolution of the joint pdf of velocity, dissipation, and other scalars is modeled and solved using a Lagrangian viewpoint. In the pdf transport equation, the terms to be modeled are those representing the effects of viscous dissipation, the fluctuating pressure gradient, and molecular diffusion. All other processes are in closed form and need not be modeled. The solution is performed by a Monte Carlo algorithm. In the boundary-layer algorithm used here, the joint pdf at each step in the x -direction is represented by a large number, N , of notional or modeled particles. At the axial position x , each particle has the position $\underline{x}^*(x)$, velocity $\underline{U}^*(x)$, relaxation rate or frequency $\omega^*(x)$, and a scalar value $c^*(x)$. The dissipation model^{16,18} is, in fact, expressed in terms of ω^* ($\equiv \epsilon^* / k$) rather than in terms of the particle dissipation ϵ^* (the tilde as in k , denotes ω -weighted means). The scalar c^* is a passive scalar with no source terms (i.e., c^* is held constant), and is used to tag particles by their jet of origin. In the general step from x to $x + \Delta x$, each particle evolves over a time interval Δt^* given by:

$$\Delta t^* = \Delta x / U^*_1. \quad (1)$$

The particle velocity and relaxation rate evolve by coupled stochastic equations described in the next section. Means and other correlations are extracted from the solution by forming sums of particle properties within spatial bins and fitting cubic B-splines to these sums.

The Stochastic Velocity-Dissipation Model

The details on the construction of the model and the choice of constants are discussed extensively by Pope and Chen¹⁶ and Pope.¹⁸ The following notation is used in the description of the models. The density is constant in the present study and is denoted by ρ . The Eulerian instantaneous velocity at position \mathbf{x} and time t , $\mathbf{U}(\mathbf{x}, t)$, is written in terms of its mean $\langle \mathbf{U}(\mathbf{x}, t) \rangle$ and fluctuation $\mathbf{u}(\mathbf{x}, t)$ as:

$$\mathbf{U} = \langle \mathbf{U} \rangle + \mathbf{u}. \quad (2)$$

According to the model for inhomogeneous flows, the increment to ω^* in the time interval dt is given by (note: angled brackets denote means):

$$d\omega^* = -\omega^* \langle \omega \rangle (S_\omega + C_\chi \Omega) dt + \langle \omega \rangle^2 h dt + \omega^* (2C_\chi \langle \omega \rangle \sigma^2)^{1/2} dW, \quad (3)$$

where

$$\Omega = \ln \left(\frac{\omega^*}{\langle \omega \rangle} \right) - \left\langle \frac{\omega}{\langle \omega \rangle} \ln \frac{\omega}{\langle \omega \rangle} \right\rangle, \quad (4)$$

and dW is a Weiner process with properties $\langle dW \rangle = 0$ and $\langle dW dW \rangle = dt$. The constants in Equation 3 have been assigned¹⁶ the values $C_\chi = 1.6$ and $\sigma^2 = 1.0$. According to the model (Equation 3) the Eulerian mean relaxation rate $\langle \omega \rangle$ evolves by

$$\frac{d\langle \omega \rangle}{dt} = -\langle \omega \rangle^2 (S_\omega - h). \quad (5)$$

The term due to h in Equation 5 is a result of the extension of the model to inhomogeneous flows and is zero in homogeneous turbulence. The term h (described in detail by Pope¹⁸) involves a constant $C_{\omega 3}$ with a suggested value of $C_{\omega 3} = 1.0$. In the present study, the change in the value of $C_{\omega 3}$ over a range of 0.0 to 5.0 produced no appreciable differences in the results obtained. While more investigation is needed to determine the magnitude of $C_{\omega 3}$, the term due to h played an insignificant role in the present calculations for the values of $C_{\omega 3}$ used. A major role of the term $h \langle \omega \rangle^2$ is to increase the value of ω^* for a nonturbulent particle ($\omega^* = 0$) and make it turbulent ($\omega^* > 0$) when it is

entrained into a turbulent region ($\langle \omega \rangle > 0$). In the present study, the entire flow was assumed to be turbulent with $\omega^* > 0$ for all particles. Nevertheless, $h \langle \omega \rangle^2$ is an additional source term for the $\langle \omega \rangle$ equation in the (non-Gaussian) turbulent region and can affect the results if $C_{\omega 3}$ is chosen large enough.

A model for S_ω that is consistent with the $k-\epsilon$ model (and the model for $\langle \omega \rangle$ used previously^{12,21}) is:¹⁶

$$S_\omega = -C_{\omega 1} S_{ij} S_{ij} / \langle \omega \rangle + C_{\omega 2}, \quad (6)$$

where

$$S_{ij} = \frac{1}{2} \left(\frac{\partial \langle U_i \rangle}{\partial x_j} + \frac{\partial \langle U_j \rangle}{\partial x_i} \right). \quad (7)$$

It should be noted that with the stochastic velocity-dissipation model, there is no need to restrict the specification of S_ω in terms of $\langle \omega \rangle$ and the mean velocity gradients. Indeed, as more insight is gained regarding the behavior of ω^* (and $\langle \omega \rangle$), S_ω can be specified to include other correlations extracted from the joint pdf of ω and velocity. With the specification in Equation 6, the resulting equation for $\langle \omega \rangle$ (Equation 5) is:

$$\begin{aligned} \frac{d\langle \omega \rangle}{dt} &= \frac{\partial \langle \omega \rangle}{\partial t} + \langle U_i \rangle \frac{\partial \langle \omega \rangle}{\partial x_i} + \frac{\partial \langle u_i \omega \rangle}{\partial x_i} = \\ &C_{\omega 1} S_{ij} S_{ij} - C_{\omega 2} \langle \omega \rangle^2 + h \langle \omega \rangle^2. \end{aligned} \quad (8)$$

The values of $C_{\omega 1}$ and $C_{\omega 2}$ were varied over the ranges 0.03 to 0.1 and 0.60 to 0.92, respectively, in the present study. The set $C_{\omega 1} = 0.04$ and $C_{\omega 2} = 0.70$ was found to result in the best agreement with data in the present study. These values are still considered to be tentative until the model is validated against several more flows. The values $C_{\omega 1} = 0.04$ and $C_{\omega 2} = 0.09$ were used by Pope¹⁸ for self-similar flows. In that study, the value of $C_{\omega 1}$ was chosen to yield the correct value of the von Karman constant ($\kappa = 0.4$) in the constant-stress wall layer calculations, and the value of $C_{\omega 2}$ was chosen to be consistent with the $k-\epsilon$ model and not varied.

The stochastic model for the velocity increment over a time interval dt is:¹⁸

$$dU_i^* = -\frac{1}{\rho} \frac{\partial \langle P \rangle}{\partial x_i} dt + D_i dt + (C_0 \bar{k} \omega^*)^{1/2} dW_i, \quad (9)$$

where

$$D_i = -\left(\frac{1}{2} + \frac{3}{4} C_o\right) \langle \omega \rangle (\tilde{k}/k) u_i^* + G_{ij}^* u_j^* - \frac{3}{4} C_o \left[\tilde{A}_{ij}^{-1} (\omega^* u_j^* - \langle \omega u_j \rangle) - (\tilde{k}/k) A_{ij}^{-1} \langle \omega \rangle u_j^* \right], \quad (10)$$

$$u_i^* = U_i^* - \langle U_i \rangle, \quad (11)$$

and

$$A_{ij} = 3 \langle u_i u_j \rangle / \langle u_k u_k \rangle. \quad (12)$$

The mean pressure is $\langle P \rangle$, D_i is the drift term, A_{ij} is the normalized Reynolds stress tensor and dW_i is an isotropic Weiner process, independent of that in Equation 3. In general, G_{ij}^* is a second-order tensor function of the Reynolds stresses and mean velocity gradients. The choice $G_{ij}^* = 0$, made here and in References 18 and 20, results in the evolution equation¹⁸ of the Reynolds stresses (derived from Equation 9) having the same form as the Rotta's model in conventional Reynolds-stress closure. For the Kolmogorov constant C_o , the value $C_o = 3.5$ recommended by Pope and Chen¹⁶ is used.

Method Based on Transport Model for $\langle \omega \rangle$ ($\langle \omega \rangle$ -Model)

Before the development of the stochastic velocity-dissipation model, some previous studies^{12,15} have used a pdf method based on a transport model for $\langle \omega \rangle$, henceforth referred to as the $\langle \omega \rangle$ -model. This model is also consistent with the k - ϵ model and can be derived from the equations for k and $\langle \epsilon \rangle$ with a remodeling of the turbulent convection term. The equation for $\langle \omega \rangle$ from this model is:

$$\frac{\partial \langle \omega \rangle}{\partial t} + \langle U_i \rangle \frac{\partial \langle \omega \rangle}{\partial x_i} = 2C_\mu (C_{\epsilon 1} - 1) S_{ij} S_{ij} - (C_{\epsilon 2} - 1) \langle \omega \rangle^2 + \frac{C_\mu}{\sigma_\omega} \frac{\partial}{\partial x_i} \left(\frac{k}{\langle \omega \rangle} \frac{\partial \langle \omega \rangle}{\partial x_i} \right), \quad (13)$$

where the turbulent convection term is modeled by gradient diffusion:

$$-\frac{\partial \langle u_i \omega \rangle}{\partial x_i} = \frac{C_\mu}{\sigma_\omega} \frac{\partial}{\partial x_i} \left(\frac{k}{\langle \omega \rangle} \frac{\partial \langle \omega \rangle}{\partial x_i} \right). \quad (14)$$

The model constants are¹⁵ $C_\mu = 0.09$, $C_{\epsilon 1} = 1.56$, $C_{\epsilon 2} = 1.88$, and $\sigma_\omega = 1.0$. The evolution equations for $\langle \omega \rangle$ from the stochastic model (Equation 8) and the $\langle \omega \rangle$ -model (Equation 13) have the same form except that $h \langle \omega \rangle^2$ is an additional term (although small in the present study) in Equation 8 and the turbulent convection term is modeled by Equation 14 in Equation 13. However, the constant $2C_\mu(C_{\epsilon 1} - 1) = 0.1$ is significantly different from the corresponding constant $C_{\omega 1} = 0.04$, and the constant $(C_{\epsilon 2} - 1) = 0.88$ is different from $C_{\omega 2} = 0.7$. The solutions for $\langle \omega \rangle$ obtained from the two models are significantly different. On the other hand, the stochastic model for velocity based on $\langle \omega \rangle$ is also significantly different:

$$dU_i^* = -\frac{1}{\rho} \frac{\partial \langle P \rangle}{\partial x_i} dt - \left(\frac{1}{2} + \frac{3}{4} C_o \right) \langle \omega \rangle u_i^* dt + (C_o k \langle \omega \rangle)^{1/2} dW_i. \quad (15)$$

The differences between Equations 9 and 15 are that the random term (involving dW_i) in Equation 9 contains the instantaneous value ω^* rather than $\langle \omega \rangle$, and there are additional drift terms in Equation 9 (see Equation 10). Further, the value of C_o appropriate for this model (Equation 15), determined by Anand and Pope,²² is $C_o = 2.1$ (see Pope and Chen¹⁶ for further discussion on these differences). The evolution equation for $\langle u_i u_j \rangle$ resulting from Equation 15 also corresponds to Rotta's model in the conventional Reynolds stress closure.

In the present study, calculations are performed using both the stochastic model and the $\langle \omega \rangle$ -model, and the results are compared against each other and against experimental data.

Algorithm for Swirling Flows

There are no theoretical limitations for computing swirling flows with the pdf method. Extensions were made to the boundary-layer algorithm to be able to compute swirling flows. For the discussions to follow, the notation $\underline{U} \equiv (U_1, U_2, U_3) \equiv (U, V, W) \equiv (\langle U \rangle + u, \langle V \rangle + v, \langle W \rangle + w)$ is used. In addition, due to the geometry of the flow considered, polar cylindrical coordinates (x, r, θ) are used. The main extensions to the algorithm are to calculate and include the axial pressure gradient and to include all terms arising due to $\langle W \rangle \neq 0$ in calculating $S_{ij} S_{ij}$ and the (radial and) axial pressure gradients.

The mean pressure gradient is computed by integrating the mean radial (or lateral) pressure gra-

dient across the radius of the flow. The mean radial pressure gradient is given by

$$\frac{1}{\rho} \frac{\partial \langle P \rangle}{\partial r} = \frac{1}{r} (\langle W \rangle^2 + \langle w^2 \rangle - \langle v^2 \rangle - r \frac{\partial \langle v^2 \rangle}{\partial r}), \quad (16)$$

where the boundary layer assumptions (neglect of axial gradients) and axisymmetry (azimuthal gradients being zero) have been used and the mean radial velocity and its gradients are neglected. The mean pressure, as a function of r at a given x , is given by

$$\langle P(r; x) \rangle = \langle P(R_0; x) \rangle - \int_r^{R_0} \frac{\partial \langle P \rangle}{\partial r} dr, \quad (17)$$

where R_0 is the radius of the outer boundary of the jet. The mean axial pressure gradient at $x + \Delta x$, as a function of r , is then deduced by

$$\frac{\partial \langle P(r; x + \Delta x) \rangle}{\partial x} = \frac{\langle P(r; x + \Delta x) \rangle - \langle P(r; x) \rangle}{\Delta x}. \quad (18)$$

Any externally imposed axial pressure gradient can be incorporated through $\langle P(R_0; x) \rangle$ in Equation 17. In the present study, $\langle P(R_0; x) \rangle$ is taken to be constant (zero) for all x . The axial pressure gradient is important in calculating the evolution of the mean axial velocity (especially its decay on the centerline) when appreciable swirl is present in the flow.

The expression for $S_{ij} S_{ij}$ is:

$$S_{ij} S_{ij} = \frac{1}{2} \left[\left(\frac{\partial \langle U \rangle}{\partial r} \right)^2 + 2 \left(\frac{\partial \langle V \rangle}{\partial r} \right)^2 + 2 \left(\frac{\langle V \rangle}{r} \right)^2 + \left(\frac{\partial \langle W \rangle}{\partial r} - \frac{\langle W \rangle}{r} \right)^2 \right]. \quad (19)$$

Again, the terms involving $\langle V \rangle$ in Equation 19 are neglected in comparison with the other terms.

Calculations

Flow Description

Calculations are performed for a constant-density coaxial swirling jet flow for which benchmark quality data from LDV measurements have been reported by Takahashi et al.²⁰

The flow considered has a central nonswirling jet of diameter $D = 9.45$ mm, a concentric annular swirling jet of diameter $D_a = 26.92$ mm surrounded by a low velocity coflow in a test section of 150 mm diameter. All the jets are of air. The bulk-averaged axial velocities for the central jet, annulus, and coflow are 100, 20, and 4 m/s, respectively. The Reynolds number for the central jet is approximately 21,400. The swirl number is defined as the ratio of the axial flux of angular momentum to that of axial momentum divided by the outer radius:

$$S = \frac{R_0 \int_{R_i}^{R_0} \rho \langle U \rangle \langle W \rangle r dr}{R_0 \int_{R_i}^{R_0} \rho \langle U \rangle^2 r dr}. \quad (20)$$

The swirl in the annular jet is produced by a vaned swirler with a vane helix angle of 30 deg, located 96 mm upstream of the nozzle exit. The swirl number for the annular jet, S_a , based on $R_i = R = D/2$ and $R_0 = R_a = D_a/2$, calculated from measured data 1.5 mm downstream of the nozzles, is 0.41. However, the overall swirl number, S_{ov} , based on the central and annular jets (with $R_i = 0$ and $R_0 = R_a$) is 0.09 due to the large bulk axial velocity of the central jet. Since the overall swirl number is low, the inclusion of the axial pressure gradient did not have a significant effect on the results. However, with another test problem²³ with an overall swirl number of approximately 0.4, the inclusion of the axial pressure gradient was necessary to obtain the correct (measured) spreading of the mean axial velocity profile.

Initial Conditions

Initial conditions for the computations are prescribed from experimental data. The first measurement station $x = 1.5$ mm ($x/D = 0.16$) is taken as the initial plane for the calculations. The initial velocity pdf is prescribed to be joint normal with the mean and covariances taken from linearly interpolated experimental data. The initial pdf of relaxation rate for the stochastic model is taken to be log-normal [$\ln(\omega^*/\langle \omega \rangle)$ has a normal distribution with mean and variance $-\frac{1}{2}\sigma^2$ and σ^2 , respectively], in accordance with the construction of the model. The specification of the initial $\langle \omega \rangle$ profile for the stochastic model is discussed later in this section.

The initial profile of $\langle \omega \rangle$ for the $\langle \omega \rangle$ -model is derived from experimental data using the expression based on the $k-\epsilon$ model:

$$\langle \omega \rangle = -C_\mu \frac{k}{\langle uv \rangle_{eq}} \left(\frac{\partial \langle U \rangle}{\partial r} \right)_{eq}, \quad (21)$$

where equivalent velocity gradient and shear stress are given by:

$$\left[\frac{\partial \langle U \rangle}{\partial r} \right]_{eq} = \left[\left(\frac{\partial \langle U \rangle}{\partial r} \right)^2 + \left(\frac{\partial \langle W \rangle}{\partial r} - \frac{\langle W \rangle}{r} \right)^2 \right]^{1/2}, \quad (22)$$

and

$$\langle uv \rangle_{eq} = (\langle uv \rangle^2 + \langle uw \rangle^2)^{1/2}. \quad (23)$$

The initial $\langle \omega \rangle$ profile was also specified from Equation 21 with the assumption of local equilibrium of turbulence energy in the shear layer that yields $\langle uv \rangle_{eq} = \sqrt{C_\mu} k$ so that:

$$\langle \omega \rangle = \sqrt{C_\mu} \left| \left(\frac{\partial \langle U \rangle}{\partial r} \right)_{eq} \right|. \quad (24)$$

Although Equations 21 and 24 result in slightly differing profiles of initial $\langle \omega \rangle$, both specifications produced nearly the same results at the downstream stations. For the results with the $\langle \omega \rangle$ -model reported here, the specification in Equation 24 was used.

The specification of $\langle \omega \rangle$ for the stochastic model needs some clarification. The production of $\langle \omega \rangle$ in the stochastic model, controlled by $C_{\omega 1} = (0.04)$ (Equation 6), is only 40% of the production with the $\langle \omega \rangle$ model [Equation 13, $2C_\mu (C_{\epsilon 1} - 1) = 0.1$]. The dissipation of $\langle \omega \rangle$ is also lower in the stochastic model, but is about 80% of that with the $\langle \omega \rangle$ -model [$C_{\omega 2} = 0.70$ versus $(C_{\epsilon 2} - 1) = 0.88$]. Hence, with the two models producing nearly the same velocity statistics, the stochastic model will yield lower values of $\langle \omega \rangle$, especially in the near-nozzle region where production is dominant due to large velocity gradients. This fact is borne out by the results presented in the next section. With the specification of the same inlet $\langle \omega \rangle$ for both the models, the stochastic model yielded lower $\langle \omega \rangle$ (by about 30%) than the $\langle \omega \rangle$ -model at the downstream locations ($x/D = 0.5$ to 10 approximately). The agreement with data of the turbulent correlations close to the nozzle ($x/D = 1.06$ and 2.65 sta-

tions) was poorer. In particular the turbulent kinetic energy was lower than in the experiments in this region. This would have an effect on the results downstream, especially the spreading rate. The results suggested that the appropriate value of inlet $\langle \omega \rangle$ for the stochastic model is about 70% of the value used for the $\langle \omega \rangle$ model, keeping in mind that the stochastic model has fluctuations in ω and noting the differences in the velocity models discussed previously. Hence the inlet $\langle \omega \rangle$ for the stochastic model is specified to be 0.7 times the value obtained from Equation 24. Again, the alternative specification of 0.7 times the value obtained from Equation 24 produced nearly the same results.

To utilize the opportunity provided by the stochastic model to specify additional initial conditions based on joint velocity-relaxation rate statistics, initial conditions on $\langle v\omega \rangle$ were specified such that the correlation coefficient for $\langle v\omega \rangle$ is the negative (from wall boundary-layer considerations) of that of $\langle uv \rangle$. Although, this specification did not have a major effect on the results, it underscores the fact that more information is contained in and can be supplied to the stochastic model.

Conditional Statistics

As mentioned previously, LDV measurements for the flow were made by seeding individual jets one at a time. The complete flow field would be mapped by seeding a particular jet and the procedure would be repeated for the remaining jets. The experiments were shown to be repeatable. This technique measures the conditional pdfs (i.e., conditional upon the jet of origin) and avoids errors due to velocity bias that will be significant due to the large differences in the bulk velocity among the jets. However, the unconditional pdf cannot be deduced from these measurements without the additional measurement of the fraction of time the fluid from each jet spends within the sample volume. The advantage with the pdf method is that the conditional pdfs are easily calculated in addition to the unconditional pdf. Conventional turbulence models can only calculate (a limited number of) unconditional correlations and cannot calculate conditional quantities without requiring additional modeling.

The comparison between conditional measurements and calculations sheds valuable light on the detailed performance on the model and on the dynamics of individual jets. In the present study, good agreement between calculated and measured conditional quantities also implies that the calcu-

lated unconditional quantities are correct since no additional modeling is required to derive the conditional quantities.

In the calculations, the particles are tagged at the initial plane by assigning the value of c^* to be 1, 2, or 3 depending on their jet of origin. The value of c^* does not change throughout the calculation. Conditional quantities are computed for output by forming sums over particles with the same value of c^* within a spatial cell and fitting B-splines to these sums.

Computational Parameters

The total number of particles used in the simulations is 150,000. A large number is used to reduce statistical error especially in the calculation of the third and fourth order moments (mean and second order quantities can be calculated to within a few percent accuracy with as low as 25,000 particles). The number of cells used for forming sums is 44 and the number of basis functions used for B-splines is 20.

The stochastic model calculations took approximately 38 minutes of CPU time to march from $x/D = 1.06$ to $x/D = 26.5$ (in about 540 steps) on a CRAY YMP. The $\langle\omega\rangle$ -model took about 28 minutes and 470 steps. No significant effort has been made to optimize the computer code for speed. The storage required was about 7 megawords.

Results and Discussion

The measured mean axial velocity on the centerline of the jet at the $x = 1.5$ mm station, $\langle U \rangle_{oc}$ ($=129.7$ m/s), is used for normalizing all the velocity statistics presented. The radial distance is normalized by the radius of the central jet (R) and the axial distance is normalized by the central jet diameter (D).

Measurements²⁰ were taken across the diameter of the flow. However, in the figures presented here, the data on either side of the centerline are shown on the same side. This gives an indication of the symmetry of the flow and the amount of scatter in the data. Measurements have been reported for $x/D = 0.16$ (initial plane), 1.06, 2.65, 5.29, 7.94, 15.9, and 26.5. Figure 1 shows the conditional mean axial velocities from the stochastic model at four different axial stations. The calculations are in very good agreement with data. The conditional velocities show the momentum transfer between the jets as they mix. The annular jet axial velocity is accelerated as the annular fluid moves towards

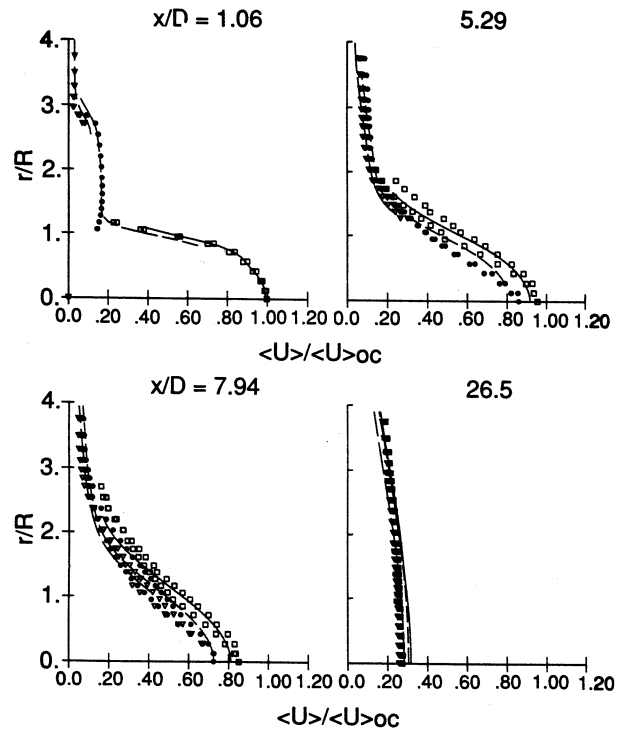


Figure 1. Radial profiles of conditional mean axial velocity from pdf (stochastic velocity-dissipation model) calculations compared against data at various axial stations. Lines denote calculations and symbols denote experimental data: solid line, \square —central jet fluid; short dashed line, \bullet —annular jet fluid; long dashed line, ∇ —coflow fluid.

the centerline and the central jet decelerates. Similarly, the coflow fluid accelerates as it moves in. The conditional velocities differ significantly from each other in the developing region, and these differences become insignificant far downstream ($x/D = 26.5$).

The corresponding mean axial velocity profiles from the $\langle\omega\rangle$ -model are shown in Figure 2. The profiles from the $\langle\omega\rangle$ -model show greater decay of the centerline velocity than those shown by the stochastic model and data. However, the conditional velocities show the same relative trends and the agreement with data over most of the radius is quite good. The spreading rate (and the centerline velocity decay) can be adjusted by changing the values of $C_{\epsilon 1}$ and $C_{\epsilon 2}$. However, tests indicated that changing the constants to get a better agreement on the spreading rate would also lower the turbulent kinetic energy (i.e., $\langle u^2 \rangle$, $\langle v^2 \rangle$, and $\langle w^2 \rangle$) and results in a poorer agreement with data for those and other turbulent correlations.

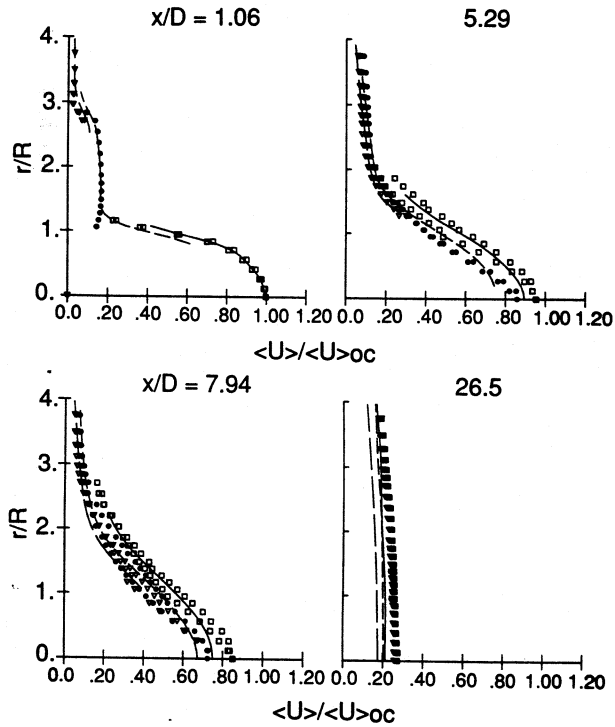


Figure 2. Radial profiles of conditional mean axial velocity from pdf ($\langle\omega\rangle$ -model) calculations compared against data at various axial stations (see Figure 1 for legend).

The profiles of $\langle\omega\rangle$ obtained from the stochastic and $\langle\omega\rangle$ -model are shown in Figure 3. As explained earlier, the $\langle\omega\rangle$ profiles, especially the peak values, from the stochastic model are considerably lower than those from the $\langle\omega\rangle$ -model in the developing region ($x/D \leq 7.94$). In this region the production of $\langle\omega\rangle$ plays a major role due to the large mean velocity gradients. The production is lower in the stochastic model due to the choice of the constants. Further downstream, production is less and the dissipation of $\langle\omega\rangle$ plays a significant role. Since the dissipation is lower in the stochastic model than in the $\langle\omega\rangle$ -model it can be seen that the $\langle\omega\rangle$ values are higher for the stochastic model at $x/D = 26.5$. In fact, the two profiles crossover at about $x/D = 16$.

The profiles of the mean swirl velocity are shown in Figure 4. The decay of the swirl velocity is well predicted at all stations including the downstream stations not shown here. The increase in swirl velocity of the central jet and coflow fluids as they move towards the annular swirling jet is clearly depicted by both the measured and calculated profiles. The profiles of $\langle W \rangle$ calculated by the $\langle\omega\rangle$ -model are also in good agreement with

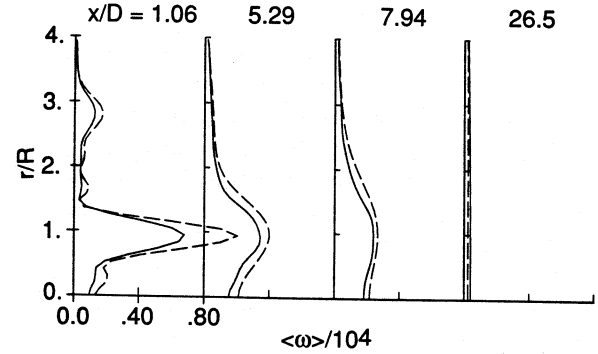


Figure 3. Profiles of mean relaxation rate $\langle\omega\rangle$ from stochastic model calculations (solid lines) compared with those from $\langle\omega\rangle$ -model calculations (dashed lines) at various axial stations.

data. The negative values of $\langle W \rangle$ shown by data at $x/D = 5.29$ and 7.94 are nonphysical and indicative of some experimental error.

Since most significant differences among the conditional quantities exist in the near nozzle region, $x/D \leq 7.94$, only selected stations in this region are shown, in the interest of clarity, in the figures to follow. The results are in good agreement with data at all stations. The profiles of turbulent kinetic energy from the stochastic model are shown in Figure 5 for $x/D = 5.29$ and 7.94 .

Figure 6 shows the unconditional and conditional mean axial velocity and turbulent kinetic energy at $x/D = 5.29$. The unconditional mean velocity lies within the conditional velocities at any given radius since:

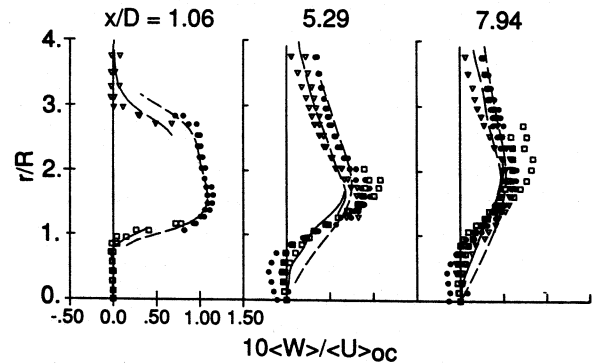


Figure 4. Profiles of conditional mean swirl velocity $\langle W \rangle$ from stochastic model calculations compared against data (see Figure 1 for legend).

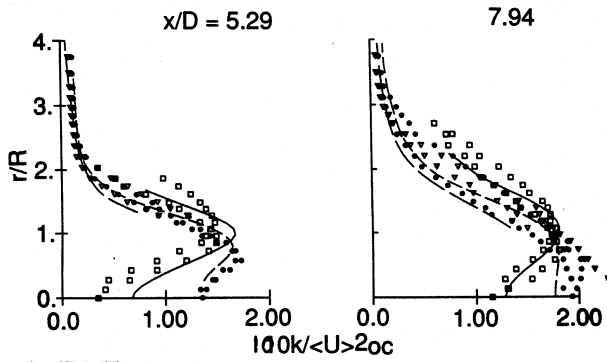


Figure 5. Profiles of conditional turbulent kinetic energy from stochastic model calculations compared against data (see Figure 1 for legend).

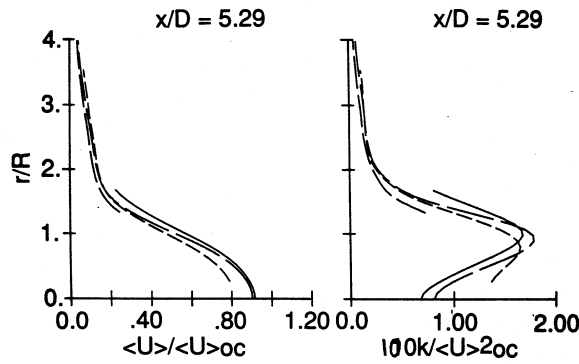


Figure 6. Profiles of conditional and unconditional mean axial velocity and turbulent kinetic energy at $x/D = 5.29$ from stochastic model calculations. Solid line—jet fluid; short dashed line—annular jet fluid; long dashed line—coflow; extra long dashed line—unconditional.

$$\langle U \rangle = \gamma_j \langle U \rangle_j + \gamma_a \langle U \rangle_a + \gamma_c \langle U \rangle_c \quad (25)$$

where the subscripts j , a , and c denote the central jet, annular jet, and coflow, respectively, and γ is the fraction of the time that the fluid from the particular jet is found at the measurement location (note that γ s are less than unity and add up to unity). However, the unconditional turbulent correlations, in general, need not lie within the conditional quantities. Expressions similar to Equation 25 can be derived for each of the correlations that will have, in addition to a linear combination of the conditional correlations, terms involving differences between the conditional mean velocities and other conditional quantities. It is easier to visualize that while the conditional fluctuations are calculated from the corresponding conditional mean, the unconditional fluctuations are with respect to the unconditional mean. For

example, in a region where the conditional velocities are significantly different, the root mean square (rms) fluctuation about the unconditional mean can be significantly larger than the rms fluctuations about the respective conditional means. This fact is illustrated by the kinetic energy profiles in Figure 6.

The kinetic energy profiles from the $\langle \omega \rangle$ -model (not shown here) are also in good agreement with data, but some differences in the details exist between the results from the two models as illustrated by the next two figures. Figures 7 and 8 show the conditional axial velocity variance from the stochastic and $\langle \omega \rangle$ -models respectively. Both models produce results that have the same level of agreement with data. However, the shift in the location of the peaks for the central and annular jets is better captured by the stochastic model than the $\langle \omega \rangle$ -model. This may be due to the fact that the turbulent transport of ω is modeled (by gradient diffusion) in the $\langle \omega \rangle$ -model while it is not modeled with the stochastic model.

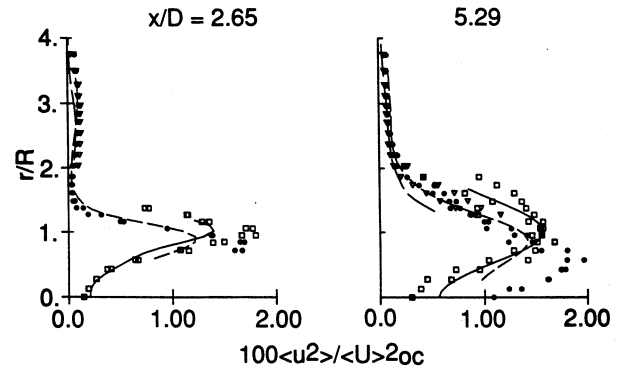


Figure 7. Profiles of conditional axial velocity variance from stochastic model calculations compared against data (see Figure 1 for legend).

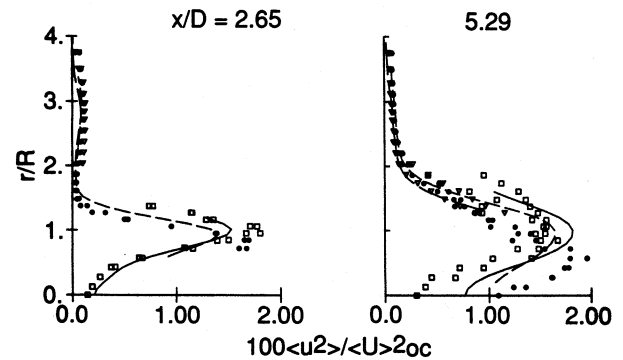


Figure 8. Profiles of conditional axial velocity variance from $\langle \omega \rangle$ -model calculations compared against data (see Figure 1 for legend).

This discrepancy in the $\langle u^2 \rangle$ profile is further amplified in the $\langle u^2 v \rangle$ profiles shown in Figures 9 and 10. The quantity $\langle u^2 v \rangle$ can be interpreted as the radial turbulent flux of $\langle u^2 \rangle$. The quantity $\langle u^2 v \rangle$ will have opposite signs on either side of the location (approximately) of the peak of $\langle u^2 \rangle$ since turbulence will disperse the peak in opposite directions from the peak. Figure 9 shows that the stochastic model shows good agreement with data while the $\langle \omega \rangle$ -model calculations are not in as good an agreement (Figure 10).

One can draw an analogy between $\langle u^2 v \rangle$ (the transport of the velocity variance $\langle u^2 \rangle$ in the v -direction) and $\langle \phi^2 v \rangle$ (the transport of $\langle \phi^2 \rangle$, variance of a scalar Φ in the v -direction). It is important to calculate scalar transport (both mean and fluctuation of the scalar) accurately, especially in reacting flows, since it significantly affects local heat release rates. It is even more critical when there is mixing between different streams (such as fuel and oxidizer in diffusion flames).

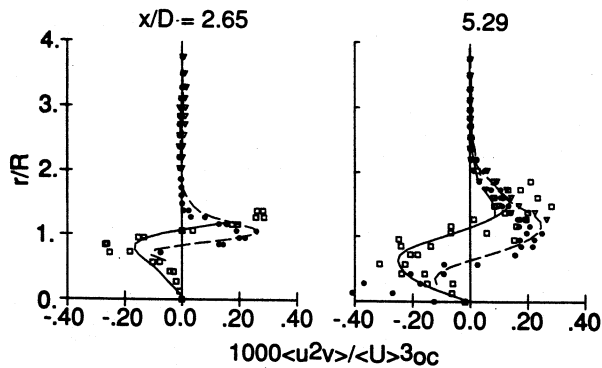


Figure 9. Profiles of (conditional) triple correlation $\langle u^2 v \rangle$ from stochastic model calculations compared against data (see Figure 1 for legend).

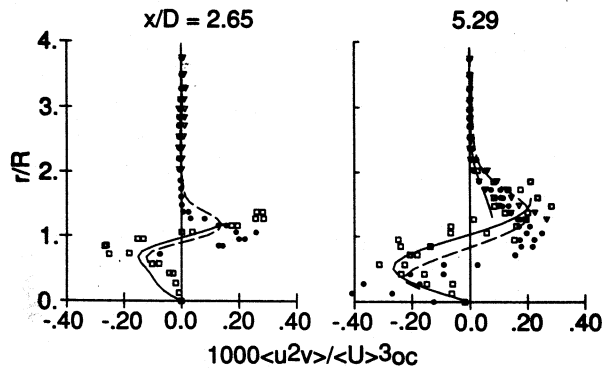


Figure 10. Profiles of (conditional) triple correlation $\langle u^2 v \rangle$ from $\langle \omega \rangle$ -model calculations compared against data (see Figure 1 for legend).

In Reynolds-stress closures, all third-order correlations (such as $\langle u^2 v \rangle$) are modeled, usually by gradient diffusion. In the present study, the flow under consideration was calculated using the RSM of Daly and Harlow²⁴ that is widely used. The details of the code and models used are presented in Reference 25. The model for $\langle u^2 v \rangle$ is:

$$\langle u^2 v \rangle = -C_s \frac{k}{\langle \varepsilon \rangle} \langle v^2 \rangle \frac{\partial \langle u^2 \rangle}{\partial r}, \quad (26)$$

where $C_s = 0.22$. The profile of (unconditional) $\langle u^2 v \rangle$ calculated from Equation 26 with the right-hand side quantities taken from the Reynolds-stress calculations (short dashed line) is compared against the unconditional $\langle u^2 v \rangle$ profile from the stochastic model calculations (solid line) in Figure 11. The comparison shows that the RSM calculations severely underpredict the transport of $\langle u^2 \rangle$ especially at the stations close to the nozzle. The magnitude of $\langle u^2 v \rangle$ is lower because the RSM calculations also grossly underpredict $\langle u^2 \rangle$ in this region. In addition the $\langle u^2 v \rangle$ profiles from the RSM calculations change sign at a different radial location than the pdf calculations since the peaks of $\langle u^2 \rangle$ are also shifted in the RSM calculations. These differences get larger further downstream. A better test of the gradient diffusion hypothesis would be to use the pdf results for the right-hand side in Equation 26. These profiles (long dashed lines in Figure 11) also show differences both in magnitude and the location where the profiles change sign. Though these discrepancies are not dramatic for the flow considered here, they underscore the fact that the gradient diffusion hypothesis

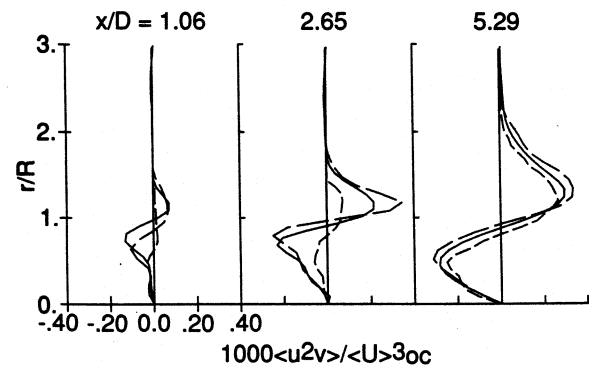


Figure 11. Profiles of (unconditional) triple correlation $\langle u^2 v \rangle$ from stochastic model calculations (solid line); from Reynolds-stress model (Equation 26) using results from Reynolds-stress closure calculations (short dashed line); and from model (Equation 26) using results from stochastic model calculations (long dashed line).

could lead to different results and in the case of reacting flows where counter-gradient diffusion has been demonstrated^{27,28} the results would be erroneous.

It should be noted that even with the scalar pdf method^{2,26} in which the joint pdf of scalars only is considered, the turbulent flux of the scalar pdf is modeled by gradient-diffusion. While the scalar-pdf method is a useful tool for the development of reduced reaction mechanisms, since reaction still appears in closed form in the method, the full potential of the pdf method can only be realized by the velocity-scalar joint pdf method.

Figure 12 shows the conditional $\langle u^3 \rangle$ profiles at $x/D = 2.65$ and 5.29 . The dramatic differences between the conditional quantities is well predicted by the calculations. The results from the $\langle \omega \rangle$ -model show similar discrepancies as seen for $\langle u^2 v \rangle$. Figure 13 shows the (conditional) fourth order correlation $\langle w^4 \rangle$ from the stochastic model at $x/D = 5.29$ and 7.94 . Considering that fourth or-

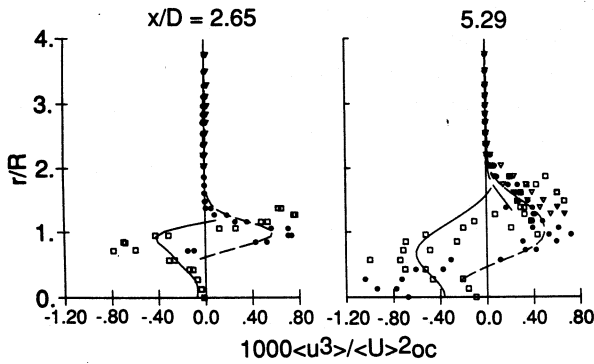


Figure 12. Profiles of conditional $\langle u^3 \rangle$ from stochastic model compared against data (see Figure 1 for legend).

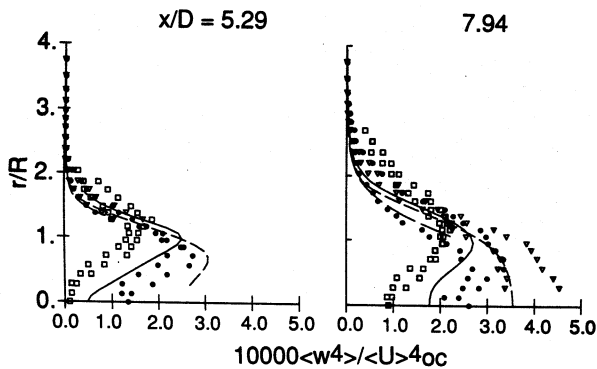


Figure 13. Profiles of (conditional) fourth-order correlation $\langle w^4 \rangle$ from stochastic model calculations compared against data (see Figure 1 for legend).

der conditional statistics are being measured and computed, the results are in very good agreement with data. The corresponding profiles for the $\langle \omega \rangle$ -model are shown in Figure 14. These profiles are also in good agreement with data. However the radial separation between the peak locations for the central jet and annulus at $x/D = 5.29$ are better predicted by the stochastic model.

Conclusions

Swirling flow calculations have been made with the pdf method. The newly developed stochastic velocity-dissipation model has been validated against benchmark quality data from a coaxial swirling jet flow. Detailed comparisons between measured and calculated conditional means and correlations up to fourth order have been made. The calculations are in very good agreement with data. The present study suggests the values $C_{\omega 1} = 0.04$ and $C_{\omega 2} = 0.7$ for the two constants that significantly affect the evolution of the mean relaxation rate $\langle \omega \rangle$.

Swirling flows were calculated for the first time using the pdf method. While extensions to the algorithm were made to include the axial pressure gradient and additional terms due to nonzero mean swirl velocity, no specific modifications were made to the ω^* -equation or elsewhere on account of swirl.

Calculations were also made with the pdf method using a transport model for $\langle \omega \rangle$. These results are also in reasonably good agreement with data, although the stochastic model better predicts some of the details of turbulent transport.

The calculated results from the stochastic model were compared against gradient-diffusion

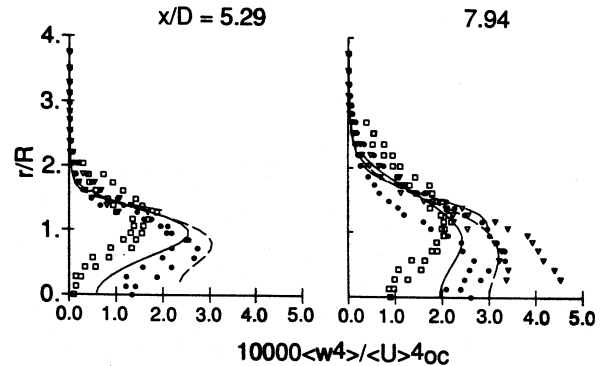


Figure 14. Profiles of (conditional) fourth order correlation $\langle w^4 \rangle$ from $\langle \omega \rangle$ -model compared against data (see Figure 1 for legend).

models used by conventional Reynolds-stress closures, and the latter were found to be deficient. By extension, the scalar pdf method is also subject to the same limitations since gradient diffusion modeling is used for turbulent transport of the scalar pdf.

The pdf model used, with $G_{ij}^a = 0$ is not very sophisticated in comparison with available Reynolds-stress closures. It corresponds to Rotta's model with no rapid pressure terms. It is remarkable, therefore, that this level of agreement with data is achieved even with this simple choice. Clearly, a more general model for G_{ij}^a should be investigated in the future.

The stochastic velocity-dissipation model provides complete closure for the joint velocity-scalar pdf method and eliminates the need to supply a time scale for the solution of the pdf transport equation. The stochastic model also contains more information than that based on $\langle \omega \rangle$, and allows the flexibility to build in more information than currently used in further developing the model.

Acknowledgment

This work is sponsored by the U.S. Air Force, Wright Laboratories, under contract F33615-87-C-2821 to Allison Gas Turbine, as part of a joint Air Force - Allison - University of Dayton Research Institute (UDRI) program. We would like to thank the Air Force Technical Monitors, Dr. Mel Roquemore and Mr. Jeff Stutrud, for their support and discussions, and Dr. Fumi Takahashi of UDRI for the experimental data and related discussions. We gratefully acknowledge the grant from NASA, Lewis Research Center for the use of the super-computing resources of the National Aerodynamic Simulation System. We also would like to thank Dr. Mohammad Nikjooy for useful discussions and providing the code for the Reynolds-stress model calculations.

References

1. S. B. Pope, *Twenty-Third Symposium (International) on Combustion*, The Combustion Institute, Pittsburgh, 591, 1990.
2. S. B. Pope, *Progress in Energy and Combustion Science*, 11, 119, 1985.
3. M. S. Anand, S. B. Pope, and H. C. Mongia, *Turbulent Reactive Flows*, Lecture Notes in Engineering, 40, Springer-Verlag, Berlin, 672, 1989.
4. M. S. Anand, S. B. Pope, and H. C. Mongia, *CFD Symposium on Aeropropulsion*, NASA Lewis, Cleveland, OH, NASA CP-3078, 347, 1990.
5. D. C. Haworth and S. H. El Tahry, *Seventh Symposium on Turbulent Shear Flows*, Stanford University, p. 13.1, 1989.
6. D. C. Haworth and S. H. El Tahry, *AIAA Journal*, 29, 208, 1991.
7. M. T. Abujela and D. G. Lilley, AIAA-84-0441.
8. S. B. Pope, *Turbulent Shear Flows 3*, Eds. L. J. S. Bradbury et al, Springer-Verlag, Berlin, 113, 1982.
9. D. C. Haworth and S. B. Pope, *Physics of Fluids*, 30, 1026, 1987.
10. S. B. Pope and S. M. Correa, *Twenty-First Symposium (International) on Combustion*, The Combustion Institute, Pittsburgh, 1341, 1986.
11. S. Tiang, A. R. Masri, and S. B. Pope, (Submitted for Publication) 1992.
12. M. S. Anand, S. B. Pope, and H. C. Mongia, *Seventh Symposium on Turbulent Shear Flows*, Stanford University, p. 3.3, 1989.
13. W. P. Jones and B. E. Launder, *International Journal of Heat and Mass Transfer*, 15, 301, 1972.
14. B. E. Launder and D. B. Spalding, *Mathematical Models of Turbulence*, Academic Press, New York, 1972.
15. M. S. Anand, AIAA-90-1856.
16. S. B. Pope and Y. L. Chen, *Physics of Fluids A*, 2, No. 8, 1437, 1990.
17. P. K. Yeung and S. B. Pope, *Journal of Fluid Mechanics*, 104, 311, 1981.
18. S. B. Pope, *Physics of Fluids A*, 3, No. 8, 1991. (See also Erratum, S. B. Pope, *Physics of Fluids A*, 4, No. 5, 1992)
19. A. T. Norris and S. B. Pope, *Eighth Symposium on Turbulent Shear Flows*, Stanford University, p. 31-2, 1991.
20. F. Takahashi, M. D. Vangsness, and V. M. Belovich, AIAA-92-0580.
21. D. C. Wilcox, *AIAA Journal*, 26, No. 11, 1299, 1988.
22. M. S. Anand and S. B. Pope, *Turbulent Shear Flows 4*, Eds. L. J. S. Bradbury et al, Springer-Verlag, Berlin, 46, 1985.
23. J. P. Sislian and R. A. Cusworth, UTIAS Report No. 281, University of Toronto, Toronto, 1984.
24. B. J. Daly and H. F. Harlow, *Physics of Fluids*, 13, 2634, 1970.
25. M. Nikjooy and H. C. Mongia, *International Journal of Heat and Fluid Flow*, 12, No. 1, 12, 1991.
26. J. Y. Chen, W. Kollmann, and R. W. Dibble, *Combustion Science and Technology*, 64, 315, 1989.
27. P. A. Libby, *Progress in Energy and Combustion Science*, 11, 83, 1985.
28. M. S. Anand and S. B. Pope, *Combustion and Flame*, 67, 127, 1987.